Nanoscale Res Lett (2009) 4:1135–1140
DOI 10.1007/s11671-009-9367-x

NANO EXPRESS

Considerable Enhancement of Field Emission of SnO_2 Nanowires by Post-Annealing Process in Oxygen at High Temperature

J. B. Wang · K. Li · X. L. Zhong · Y. C. Zhou · X. S. Fang · C. C. Tang · Y. Bando

Received: 13 February 2009 / Accepted: 28 May 2009 / Published online: 24 June 2009

Abstract The field emission properties of SnO_2 nanowires fabricated by chemical vapor deposition with metallic catalyst-assistance were investigated. For the as-fabricated SnO_2 nanowires, the turn-on and threshold field were 4.03 and 5.4 V/μm, respectively. Considerable enhancement of field emission of SnO_2 nanowires was obtained by a post-annealing process in oxygen at high temperature. When the SnO_2 nanowires were post-annealed at 1,000 °C in oxygen, the turn-on and threshold field were decreased to 3.77 and 4.4 V/μm, respectively, and the current density was increased to 6.58 from 0.3 mA/cm^2 at the same applied electric field of 5.0 V/μm.

Keywords SnO_2 nanowires · Chemical vapor deposition · Field emission · Annealing

Introduction

SnO_2 is an important *n* type wide-band gap ($E_{g.} = 3.6$ eV, at 300 K) semiconducting material, which exhibits extensive applications in the fields of gas sensors, transparent conducting electrodes, transistors, electrode materials, catalysis, solar cells, and optoelectronic devices [1–5]. Recently, various SnO_2 nanostructures [6–9] have been proved to be promising candidates for field emission-based flat panel displays due to their characteristic properties of high physical and chemical stability and causticity resistance, compared with ZnO nanostructures and carbon nanotubes. These excellent demonstrations of electron emission from SnO_2 nanostructures have opened the door to a new area of applications of these materials for the production of efficient cold cathodes. In order to develop efficient and controllable field emission devices based on SnO_2 nanostructures at a lowest energy expense, effective methods to optimize their field emission properties are highly desirable to achieve the highest current density at the lowest threshold electric field. However, the researches specialized on how to enhance the field emission properties of SnO_2 nanostructures have been limited to only a few reports [10, 11]. In this paper, SnO_2 nanowires are fabricated by a chemical vapor deposition method with metallic catalyst-assistance. It is found that the post-annealing process in oxygen is an effective method for enhancing the field emission of SnO_2 nanowires.

Experimental Method

A chemical vapor deposition method with metallic catalyst-assistance was employed for the preparation of SnO_2 nanowires [7, 10]. A layer of Au (about 7 nm in the thickness) as a catalyst was first deposited on Si substrates with the area of ~8 mm^2 by DC sputtering. Commercial SnO_2 powders (99.9%) and graphite powders (99.99%) were mixed in a 3:1 molar ratio, transferred to a carnelian mortar and skived for 30 min to make the starting materials well mixed. The mixture was placed into a small quartz

J. B. Wang (✉) · K. Li · X. L. Zhong · Y. C. Zhou
Institute of Modern Physics, Xiangtan University, 411105 Xiangtan, Hunan, China
e-mail: jbwang@xtu.edu.cn

J. B. Wang · K. Li · X. L. Zhong · Y. C. Zhou
Key Laboratory of Low Dimensional Materials and Application Technology of Ministry of Education, Xiangtan University, 411105 Xiangtan, Hunan, China

X. S. Fang · C. C. Tang · Y. Bando
Nanoscale Materials Center, National Institute for Materials Science, Tsukuba 3050047, Japan

tube, and then the substrate was put near the mixture at a distance about 1.5 cm. The small quartz tube was pulled into the center of the large quartz tube furnace. During the whole reaction process, Ar (99.999%) was used as a carrier gas to create the inert atmosphere inside the furnace. When the tube furnace was pumped to 8 Torr by a mechanical pump, the starting materials were heated to 950 °C from room temperature in 30 min and kept at 950 °C for 15 min. After this process, the furnace was cooled down to room temperature in several hours. Finally, the substrate with a gray film-like production was taken out from the small quartz tube and used for analysis. The as-grown SnO_2 nanowires were post-annealed in oxygen for 1 h at 700, 850, 900, 950, and 1,000 °C, respectively.

The general morphologies of the as-fabricated SnO_2 nanowires were characterized by a scanning electron microscope (SEM, LEO-1525). Phase identification and degree of crystallinity of the samples were studied by a D/max -rA X-ray diffractometer with Cu–Kα radiation using normal θ–2θ scanning method. The microstructure and composition of the samples were studied with a JEOL JEM-2100 transmission electron microscope (TEM), a high resolution-transmission electron microscope (HR-TEM) and an energy-dispersive X-ray spectroscope (EDX) attached to the TEM instrument. Field emission measurements for SnO_2 nanowires were carried out with diode structure in a vacuum chamber at a pressure of 5×10^{-6} Torr at room temperature. The sample (as a cathode) was separated from a Cu probe anode. The voltage with an increasing step was continuously applied from a Cu probe (anode) to the sample (cathode) until a short-current was detected.

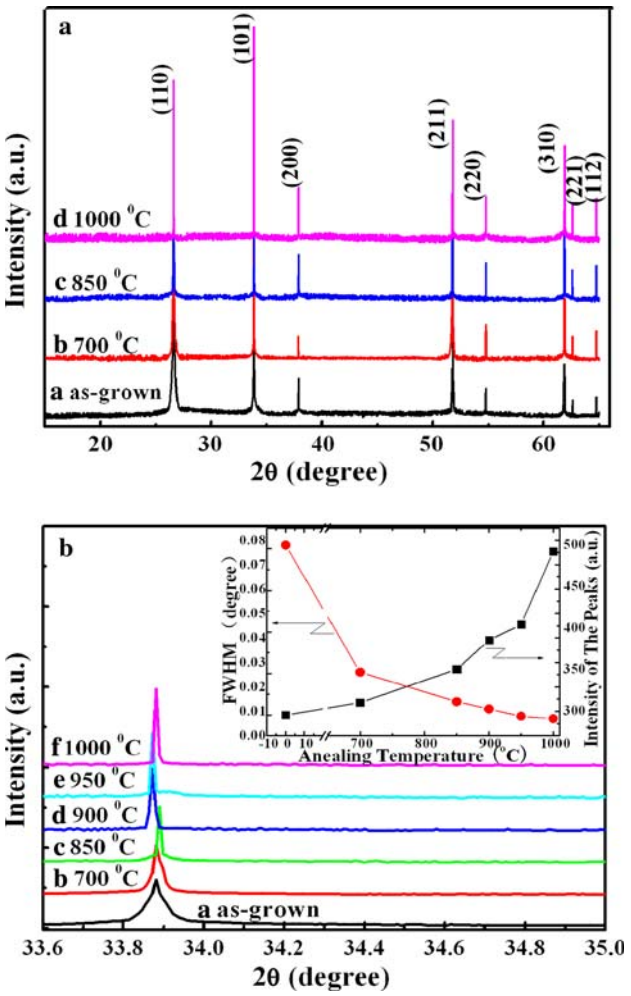

Fig. 1 **a** XRD patterns of *a* as-grown and post-annealed SnO_2 nanowires at *b* 700 °C, *c* 850 °C, and *d* 1,000 °C, respectively. **b** The (101) diffraction peak of *a* as-grown and post-annealed at *b* 700 °C, *c* 850 °C, *d* 900 °C, *e* 950 °C and *f* annealed at 1,000 °C, respectively, inset is the variation of the FWHM and the intensity of the peaks as a function of annealing temperature

Results and Discussion

Structural Analyses

The crystal structure of the as-grown SnO_2 samples was detected by XRD. Figure 1a shows XRD patterns of (a) as-grown and post-annealed SnO_2 nanowires at (b) 700 °C, (c) 850 °C and (d) 1,000 °C, respectively. All the diffraction peaks in the pattern can be indexed as a crystal structure of the tetragonal rutile SnO_2 structure with lattice constants of $a = 0.474$ nm and $c = 0.318$ nm, consistent with the standard data file (ICDD-PDF41-1445). It can be seen from Fig. 1a that the intensity of the (101) peak is much higher than those of the other peaks, indicating a growth preference in the (101) direction for the SnO_2 nanowires. Figure 1b shows the (101) diffraction peaks of the as-grown and all the post-annealed SnO_2 nanowires, and the inset shows the values of the full width at half maximum (FWHM) and the intensity of the (101) peaks as a function of annealing temperature. One can see that with increasing annealing temperature, the intensity of the (101) peaks increases, while FWHM decreases gradually, which indicates that the crystallization of the nanowires is gradually improved by a post-annealing procedure in oxygen.

Scanning electron microscope (SEM) morphologies of the fabricated nanowires are shown in Fig. 2. As shown in Fig. 2, the as-fabricated nanowires are homogeneous compact tangly and randomly extending. The length of the nanowires is more than 10 μm and the width is in the range of 30–95 nm. Note that we estimate the length of the synthesized nanowires by some low magnification SEM images in this study. For example, in Fig. 2, we use the scale bar to measure the length, in which we can easily find many nanowires with size more than 10 μm.

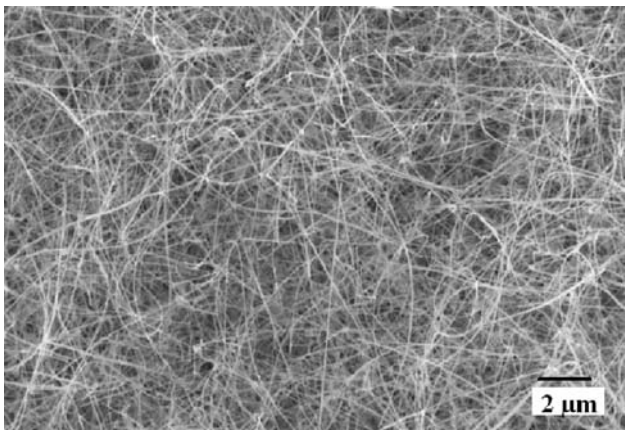

Fig. 2 SEM image of as-fabricated nanowires

The morphology and microstructure of the as-fabricated SnO_2 nanowires was performed by TEM. Figure 3a exhibits the TEM image of as-grown SnO_2 nanowires. The HR-TEM image of the selected region in (a) is shown in Fig. 3b, which indicates that the entire nanowire is a single crystal. The image of Fig. 3b shows a perfect lattice of the SnO_2 rutile structure and the measured lattice spacing is approximately 0.26 nm ascribed to the (101) plane. It is deemed that the growth preference direction of SnO_2 nanowires is the (101) direction, consistent with the XRD pattern. Energy dispersive X-ray spectroscopy (EDS) analysis is presented in Fig. 3c, which reveals the presence of Sn and O, indicating the formation of SnO_2. Some unmarked signals in the EDS spectrum come from the TEM grid used. It should be noted that the EDS data show the ratio of O to Sn is 1.51 for the as-grown nanowires, which is much lower than the stoichiometric ratio of SnO_2. But it is confirmed by both the XRD and HR-TEM image analysis that the as-grown nanowires are SnO_2 not Sn_2O_3. It is common that there are many oxygen vacancies in SnO_2 nanowires due to the lack of oxygen during the growth of nanostructures by this chemical vapor deposition method [7, 11]. Figure 3d shows that the atomic ratio of O to Sn in SnO_2 nanowires increases gradually with the increment of annealing temperature. It indicates that the oxygen vacancies in the as-grown SnO_2 nanowires are compensated by post-annealing in oxygen.

Field Emission Performance

Figure 4 shows the relation of field emission current density (J) and the applied electric field (E) measured at an anode–cathode separation of about 160 μm for the as-fabricated SnO_2 nanowires. Generally speaking, the turn-

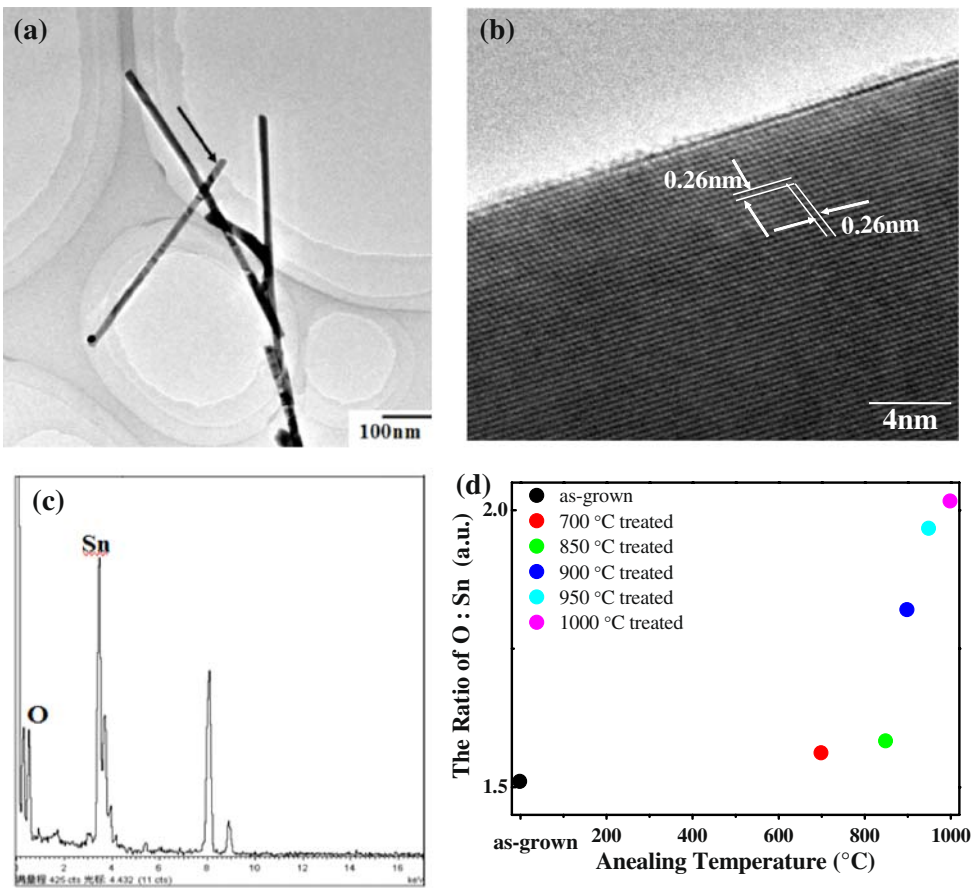

Fig. 3 **a** TEM images of SnO_2 nanowires, **b** HRTEM images of SnO_2 nanowires, **c** the EDS spectrum of SnO_2 nanowires, **d** the ratio of O to Sn in SnO_2 nanowires annealed at different temperatures

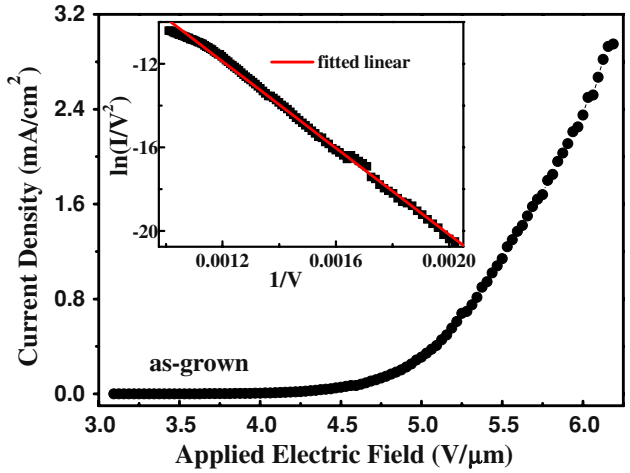

Fig. 4 Field-emission *J-E* curve for the as-grown SnO_2 nanowires. Inset is the corresponding F–N plot

on field is defined as the applied electric field where current density is distinguished from the background noise, and the threshold field is defined as the E where the J arrives at 1 mA/cm^2 [12]. From the *J-E* curve, the turn-on and threshold fields are about 4.03 and 5.4 V/μm, respectively. And the field emission current density is approximately 0.3 mA/cm^2 at the applied electric field of 5.0 V/μm.

The inset of Fig. 4 is the corresponding Fowler–Nordheim (F–N) plot. The plot goes near to a straight line, which indicates that the field emission from SnO_2 nanowires follows the F–N relationship and reveals that the field emission process is a barrier tunneling quantum mechanical process [13–15].

Usually, the classic F–N law [16] is used to describe the relationship between the field-emission-current density J and the local electric field E_{loc} to give a profound analysis of the emission properties. The F–N equation can be depicted as:

$$J = \frac{aE_{loc}^2}{\Phi}\exp\left(\frac{-b\Phi^{3/2}}{E_{loc}}\right) \quad (1)$$

where J is the field-emission-current density, Φ is the barrier height for the emission surface (the work function for SnO_2 is 4.5 eV [17]). a and b are constants with the value of 1.54×10^{-10} (A V^{-2} eV) and 6.83×10^3 (V eV$^{-3/2}$ μm^{-1}), respectively. E_{loc} represents the applied local electric field around the probe. E_{loc} could be up to hundreds or thousands times of the macroscopic electric field between the anode and the cathode. E_{loc} can be described as:

$$E_{loc} = \beta\frac{V}{d} \quad (2)$$

where V is the applied voltage, d is the distance between the anode and the cathode. β is the field enhancement factor, which reflects the ability of the emitters to enhance the applied local electric field around the probe compared to the macroscopic electric field. The value of β is related to the emitter geometry morphology, the crystal structure, and the spatial distribution of emitting centers.

From the Eqs. (1) and (2), the F–N equation could be predigested as:

$$\ln\frac{I}{V^2} = \ln\frac{aA^2\beta^2}{\Phi d} - \frac{bd\Phi^{3/2}}{\beta}\frac{1}{V} \quad (3)$$

where I is the field emission current. And then, the field enhancement factor β can be estimated by dint of the slopes S of the fitted straight lines of the F–N plots, viz. $\beta = -bd\Phi^{3/2}/S$. Consequently, the field enhancement factor β of the as-fabricated SnO_2 nanowires is 1,008.

Figure 5 shows the field emission properties of SnO_2 nanowires post-annealed in oxygen at different temperatures. These curves indicate the functions between field-emission-current density and applied electric field. One can see that excellent field emission properties of the post-annealed SnO_2 nanowires are achieved. Compared with the as-fabricated SnO_2 nanowires, the turn-on and threshold fields are decreased, and the current density is increased. When the annealing temperature is higher than 700 °C, the field emission current density increased hastily with the increment of the annealing temperature. After annealing at 1,000 °C, the turn-on and threshold fields of SnO_2 nanowires are decreased to 3.77 and 4.4 V/μm, respectively. It is noteworthy that the current density is up to 6.58 mA/cm^2 at the applied electric field of 5.0 V/μm, which is almost 22 times of that of as-fabricated SnO_2 nanowires. Hereby, post-annealing process in oxygen at high temperature is an effective method to considerably improve the field emission properties of SnO_2 nanowires.

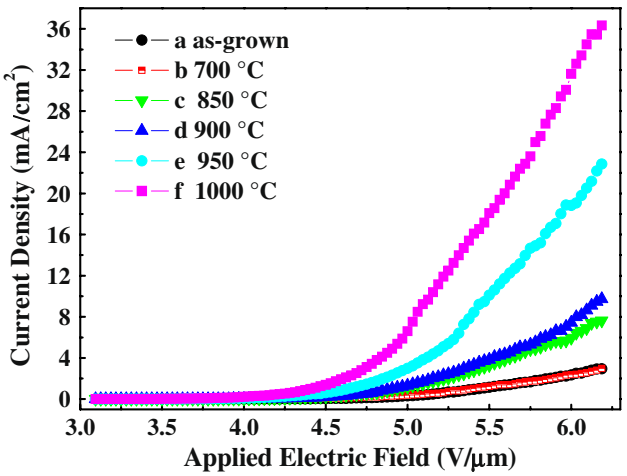

Fig. 5 Field-emission *J-E* curves for *a* as-grown and post-annealed SnO_2 nanowires in oxygen at *b* 700 °C, *c* 850 °C, *d* 900 °C, *e* 950 °C and *f* 1,000 °C, respectively

Discussion

In general, the field emission properties depend on the field enhancement factor β and the work function of the sample. The field enhancement factor depends on both the tip morphology and the density of the nanostructures. Usually, nano-structured SnO_2 with a high aspect ratio show good field emission performance, due to their much higher β value. Therefore, the shorter and thinner nanowires may be propitious to FE process and beneficial to improve the FE properties. Additionally, in the SnO_2 nanostructures case, the catalysts such as Au nanoparticles seem no significant influence of the FE performance of SnO_2 nanostructures [6, 7, 10, 18]. Table 1 summarized the FE properties of different SnO_2 nanostructures, such as hierarchical sallowlike [9], fishbone-like nanostructures [9], nanowhiskers [10], beaklike nanorods [18], and zigzag nanobelts [19]. From Table 1, one can see that FE properties of SnO_2 can be enhanced by optimizing the morphologies of SnO_2 nanostructures, but the FE current of SnO_2 nanostructures is lower than 1 mA/cm^2 (at 5 V/μm). Recently, Jang et al. [11] have found that the FE properties of SnO_2 nanowires can be improved by a post-treatment of H_2 exposure process. But the H_2 exposure treatment cannot effectively compensate oxygen vacancies generated during the growth process. Figures 1 and 3 clearly show that oxygen vacancies are effectively compensated and the perfect of crystal is improved, so the FE properties of SnO_2 nanowires annealed at high temperature in oxygen can be improved.

The main reason for the low the turn-on and threshold fields, large current density of high temperature treated SnO_2 nanowires in oxygen can be probably attributed to the following factors: the high crystalline structure and the reduction of the oxygen vacancy concentration. Generally, the high temperature annealing can greatly improve the perfect of crystal, which can be seen from Fig. 1. Thus the improvement of crystalline structure of the treated nanowires is benefit to the field emission performance of nanowires. For nanostructures of semiconductor, it is well known that surface states play an important role in influencing the carrier concentration, carrier mobility, and the effective barrier height. Therefore, these surface states can act as electron traps, forming a high potential barrier on the nanowires surface to reduce the conductivity. Thermal annealing with high temperature in oxygen could not only promote the crystalline quality of nanostructures by removing structural defects such as point defects, but also passivate the surface defects such as oxygen vacancies of SnO_2 nanowires. Importantly, our XRD data show that the crystalline quality of SnO_2 nanowires is highly promoted by high temperature annealing in Fig. 1. Meanwhile, our EDS spectrums clearly show that the increase of O atomic content with the annealing temperature increased in Fig. 3.

On the other hand, the reduction of the oxygen vacancy concentration of SnO_2 nanowires can decrease the surface barrier. Then, the Fermi level heightens and moves to the bottom of conduction band, and the carrier concentration and conductivity increase. Therefore, the work function becomes smaller and field emission property is enhanced. To quantificationally understand the influence of the annealing temperature on the work functions, the F–N plots are conducted as shown in Fig. 6. Here, the field emission factor β is considered to be the same before and after treatments, because the morphology and surface density of the nanowires are not changed very much after treatments. According to the F–N plots, the work functions are estimated in virtue of the slopes S and the field emission factors β. Figure 7 shows the work function of SnO_2 nanowires as a function of annealing temperature. As shown in Fig. 7, the work function decreases exponentially

Table 1 FE properties of different morphologies of SnO_2 nanostructures

Different morphologies	Turn-on field (Vμm^{-1})	Threshold field (Vμm^{-1})	Current density (at 5 Vμm^{-1}) mA/cm^2	References
Sallow-like	1.88	3.98	–	[9]
Fishbone-like	2.36	2.87	~1.0	[9]
Beaklike nanorods	5.8	–	–	[18]
Nanowhiskers	1.37	–	~0.1	[10]
Zigzag nanobelts	1.9	5.1	~0.9	[19]
As-grown nanowires	4.03	5.4	0.3	This paper
Nanowires post-annealed in O_2 at 1,000 °C	3.77	4.4	6.58	This paper

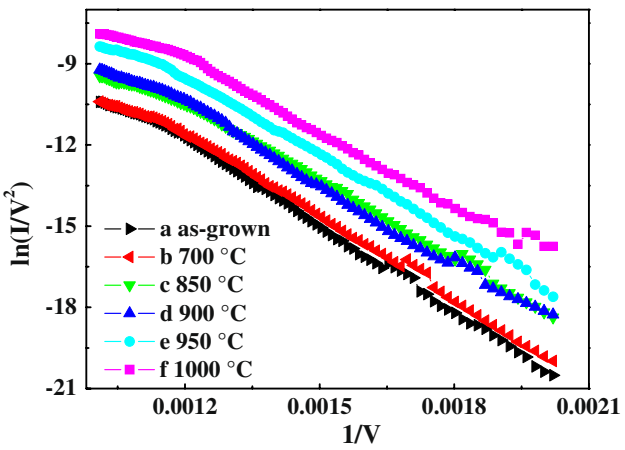

Fig. 6 F–N plots for *a* as-grown and post-annealed SnO_2 nanowires in oxygen at *b* 700 °C, *c* 850 °C, *d* 900 °C, *e* 950 °C and *f* 1,000 °C, respectively

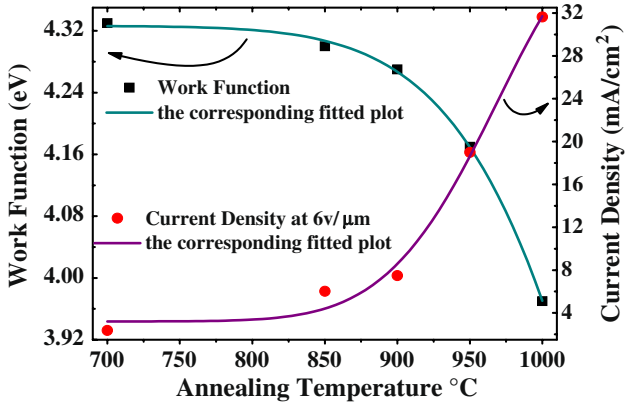

Fig. 7 The work function and corresponding current density at 6 V/μm as a function of the annealing temperature

with increasing the annealing temperature. Accordingly, the corresponding current density at 6 V/μm increases exponentially with the increment of annealing temperature, which is also shown in Fig. 7.

Conclusions

In conclusion, the homogeneous compact tangly SnO_2 nanowires were synthesised by chemical vapor deposition with metallic catalyst-assistance. The considerable enhancement of field emission from SnO_2 nanowires is observed by post-annealing the nanowires in oxygen at high temperatures. The turn-on and threshold fields of SnO_2 nanowires decreases and the current density increases with the increment of annealing temperature. The enhancement of field emission from SnO_2 nanowires is considered to be related with the reduction of the oxygen vacancy concentration in nanowires by post-annealing in oxygen at high temperature.

Acknowledgments This work was financially supported by the National Natural Science Foundation of China (Nos. 50702048 and 10525211), the Project supported by Hunan Provincial Natural Science Foundation of China (Nos. 09JJ1006), and the Specialized Research Fund for the Doctoral Program of Higher Education (No. 20070530010).

References

1. P.C. Hollamby, P.S. Aldridge, G. Moreti, R.G. Egdell, Surf. Sci. **280**, 393 (1993)
2. O.K. Varghese, L.K. Malhotra, Sens. Actuat. B **53**, 19 (1998)
3. R.H. Baughman, A.V. Zakhidov, W.A. DeHeer, Science **297**, 787 (2002)
4. S. Senda, Y. Sakai, Y. Mizuta, S. Kita, F. Okuyama, Appl. Phys. Lett. **85**, 5679 (2004)
5. X.M.H. Huang, C.A. Zorman, M. Mehregany, M.L. Roukes, Nature **421**, 496 (2003)
6. Y.J. Chen, Q.H. Li, Y.X. Liang, T.H. Wang, Appl. Phys. Lett. **85**, 5682 (2004)
7. B. Wang, Y.H. Yang, C.X. Wang, N.S. Xu, G.W. Yang, J. Appl. Phys. **98**, 124303 (2005)
8. A.C. Deshpande, P.M. Koinkar, S.S. Ashtaputre, M.A. More, S.W. Gosavi, P.D. Godbole, D.S. Joag, S.K. Kulkarni, Thin. Solid. Films. **515**, 1450 (2006)
9. Q.Y. Wang, K. Yu, F. Xu, Solid. State. Commun. **143**, 260 (2007)
10. S.H. Luo, Q. Wan, W.L. Liu, M. Zhang, Z.F. Dai, S.Y. Wang, Z.T. Song, C.L. Lin, Nanotechnology **15**, 1424 (2004)
11. H.S. Jang, S.O. Kang, Y.I. Kim, Solid. State. Commun. **140**, 495 (2006)
12. M.K. Li, D.Z. Wang, Y.W. Ding, X.Y. Guo, S. Ding, H. Jin, Mater. Sci. Eng. A **452**, 417 (2007)
13. A.G. Rinzler, J.H. Hafner, P. Nikolaev, L. Lou, S.G. Kim, D. Tomnek, P. Nordlander, D.T. Colbert, D. Ugarte, Science **269**, 1550 (1995)
14. W.A. DeHeer, A. Chatelain, D. Ugarte, Science **270**, 1179 (1995)
15. F.C.K. Au, K.W. Wang, Y.H. Tang, Y.F. Zhang, I. Bello, S.T. Lee, Appl. Phys. Lett. **75**, 1700 (1999)
16. R.H. Fowler, L.W. Nordheim, Proc. R. Soc. London, Ser. A **119**, 172 (1928)
17. J. Szuber, G. Czempik, R. Larciprete, B. Adamowicz, Sens. Actuat. B **70**, 177 (2000)
18. J.H. He, T.H. Wu, C.L. Hsin, K.M. Li, L.J. Chen, Y.L. Chueh, L.J. Chou, Z.L. Wang, Small **2**, 116 (2006)
19. J. Wu, K. Yu, L.J. Li, J.W. Xu, D.J. Shang, Y.E. Xu, Z.Q. Zhu, J. Appl. Phys. **41**, 185302 (2008)